Infrared imaging and acoustic sizing of a bubble inside a MEMS piezo ink channel

AIP | Journal of Applied Physics

Infrared imaging and acoustic sizing of a bubble inside a micro-electro-mechanical system piezo ink channel

Arjan van der Bos, Tim Segers, Roger Jeurissen, Marc van den Berg, Hans Reinten et al.

Citation: J. Appl. Phys. **110**, 034503 (2011); doi: 10.1063/1.3606567
View online: http://dx.doi.org/10.1063/1.3606567
View Table of Contents: http://jap.aip.org/resource/1/JAPIAU/v110/i3
Published by the American Institute of Physics.

Infrared imaging and acoustic sizing of a bubble inside a micro-electro-mechanical system piezo ink channel

Arjan van der Bos,[1,2] Tim Segers,[1] Roger Jeurissen,[1] Marc van den Berg,[2] Hans Reinten,[2] Herman Wijshoff,[2] Michel Versluis,[1] and Detlef Lohse[1]
[1]*Physics of Fluids Group, Department of Science and Technology, Mesa+ institute, and Burgers Center of Fluid Dynamics, University of Twente, P.O. Box 217, 7500 AE Enschede, The Netherlands*
[2]*Océ Technologies B.V., P.O. Box 101, 5900 MA Venlo, The Netherlands*

(Received 13 November 2010; accepted 29 May 2011; published online 2 August 2011)

Piezo drop-on-demand inkjet printers are used in an increasing number of applications because of their reliable deposition of droplets onto a substrate. Droplets of a few picoliters are ejected from an inkjet nozzle at frequencies of up to 100 kHz. However, the entrapment of an air microbubble in the ink channel can severely impede the productivity and reliability of the printing system. The air bubble disturbs the channel acoustics, resulting in disrupted drop formation or failure of the jetting process. Here we study a micro-electro-mechanical systems-based printhead. By using the actuating piezo transducer in receive mode, the acoustical field inside the channel was monitored, clearly identifying the presence of an air microbubble inside the channel during failure of the jetting process. The infrared visualization technique allowed for the accurate sizing of the bubble, including its dynamics, inside the intact printhead. A model was developed to calculate the mutual interaction between the channel acoustics and the bubble dynamics. The model was validated by simultaneous acoustical and infrared detection of the bubble. The model can predict the presence and size of entrapped air bubbles inside an operating ink channel purely from the acoustic response. © *2011 American Institute of Physics*. [doi:10.1063/1.3606567]

I. INTRODUCTION

Inkjet printing is the most widespread technological application of microfluidics. It is becoming increasingly popular for applications that require precise material deposition, such as the printing of electronics, displays, medical chips, solar panel printing, and even creating 3D structures.[1] Piezo drop on demand inkjet printing is becoming the favored technique for many applications, as this technique allows for the deposition of liquids with a broad range of viscosities and temperatures.[2] In order to increase the productivity of the piezo inkjet printheads, a lot of effort is put into increasing the drop repetition rate while reducing the drop size. Additionally, the applications desire a constant drop size distribution and 100% reliability. In order to fulfill this demand, research is being done on smaller and faster piezo inkjet channels.

Micro-electro-mechanical-system (MEMS) technology is widely applied in the chip industry. MEMS technology is also becoming increasingly important for future generations of inkjet printheads. With printheads produced on the wafer scale, complex designs with sub-micron details can be created in large quantities while decreasing the overall cost per nozzle. This technique has already been applied for thermal inkjet printing,[3] and more recently MEMS-based piezo inkjet printheads also have been developed.[4] Here we study a prototype printhead from Océ Technologies B.V. with an integration density of four channels per square millimeter and a drop production rate of up to 100.000 droplets per channel.

The reproducibility and reliability of an ink channel rely not only on the design of the printhead, but also on the properties of the ink, the driving waveform that actuates the channel, and the environment in which the printhead is operated. One major reliability issue in piezo inkjet printing is when an air bubble gets entrapped inside the nozzle. Especially at very high drop frequencies, the printing process becomes more susceptible to air entrapment. Entrapment can occur due to an ink film on the nozzle plate or due to dust particles around the nozzle.[5] If the actuation is continued after a bubble's entrapment, the bubble will grow due to rectified diffusion.[6–9] At the same time, a force is exerted on the bubble by the acoustic driving field inside the channel. The dominating forces are the primary Bjerknes force, which pulls the bubble into the channel, and the secondary Bjerknes force,[6–10] which pushes the bubble against the channel wall. After several thousands of actuations, the bubble will have grown to such a size that its pulsation contributes to the overall acoustic field. This results in a disturbed drop formation and, in some cases, a complete stop of the jetting process.[5,11] The only methods for restoring the nozzle's performance are to either flush the ink including the bubble or stop the actuation long enough for the bubble to dissolve due to capillary forces. These methods consume both ink and time and are therefore highly undesirable.

The geometry of the new MEMS printhead is one order of magnitude smaller than that of previously studied systems. It can be assumed that air bubbles also impede the productivity of these channels, but until now this was not confirmed because doing so requires optical access to the operating ink channel. As silicon becomes transparent at wavelengths between 1.1 μm and 6 μm (near-infrared light), it is possible

to visualize the inner channel. Although the principle of visualizing flows inside silicon devices was demonstrated in earlier research,[12–14] sizing a bubble within an unmodified printhead has not been demonstrated before.

In addition to visual characterization, attempts were also made to detect the bubble acoustically and to measure the effect of the bubble on the channel acoustics. This was done by using the piezo as sensing device. A similar technique was also applied in earlier work[11,15,16] and has proven to be a reliable technique for monitoring the onset and growth of disturbances.

In the following, two situations are studied: first, a bubble dissolving inside the channel, and second, a stable bubble oscillating in the acoustic field. The complex relations between the acoustics and the bubble dynamics are studied by means of a one dimensional acoustic model, which has proven to be fast and reliable for calculating the channel pressure and the flow rate.[16] Two-way coupling between the channel acoustics and the bubble dynamics is included in the model. A comparison of the modeled and measured acoustic signal leads to a prediction of the bubble size. The infrared measurements are then used to validate the results from the acoustic model. Finally, the model is used to predict the effect of the presence of a bubble on the ink velocity inside the nozzle.

II. GEOMETRY OF THE MEMS CHANNEL

The printhead used for this research was designed and developed by Océ Technologies B.V. in the Netherlands and is a MEMS-based design containing 320 individual channels integrated into a single chip. A schematic overview of a single channel is shown in Fig. 1. The ink is supplied from a reservoir that is placed on top of the chip. From the reservoir, the ink flows through a restriction into the actuation chamber, which is 400 μm $\times$ 400 μm $\times$ 75 μm in size. Below the actuation chamber, the ink flows into a 300 μm long feed-through with a diameter of 175 μm. At the end of the feed-through, a 75 μm thick nozzle plate is positioned. The nozzle plate consists of a pyramid shaped funnel and a cylindrical pipe with a radius of about 11 μm. To create the funnel, the nozzle wafer is etched with a KOH solution. This dissolves the silicon preferentially in the $\langle 100 \rangle$ planes,[17] resulting in a smooth surface with an angle of 54.7°.

The channel is designed such that its resonance frequency is approximately 150 kHz, allowing each individual channel to print droplets with frequencies of up to 100 kHz. The acoustic field is generated by a piezo element placed on top of the actuation chamber. The piezo is actuated with a trapezial pulse of 4 μs (1 μs rise, 2 μs high, and 1 μs fall time), driving the channel close to its resonant frequency. Applying the actuation pulse with an amplitude of 35 V results in droplets of 4 pl and a velocity of approximately 6 m/s. The ink used is not water based but a non-colored version of the CrystalPoint™ technology.[18] This hot melt ink type is printed at a temperature of 130 °C. At this temperature the viscosity of the ink is 10 mPas, the density is 1080 kg/m^3, and the surface tension is 28 mN/m.

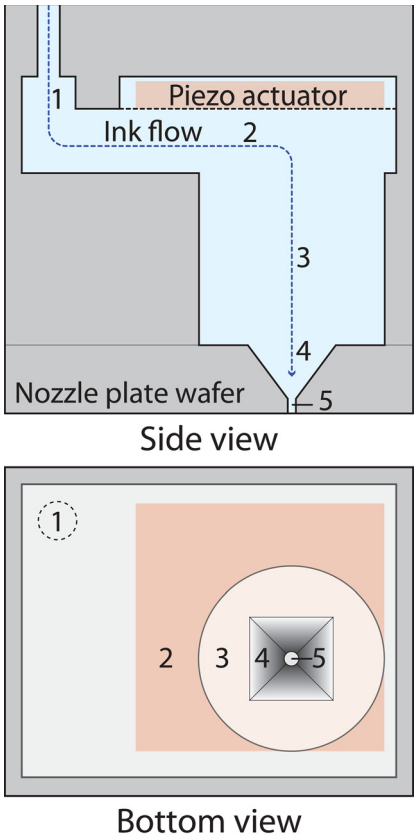

FIG. 1. (Color online) A schematic overview of the MEMS piezo inkjet channel, showing a side and bottom view. The dotted line depicts the ink-flow; the ink, coming from the reservoir, enters through a restriction (1), from which it flows into the actuation chamber (2). Below the actuation chamber, a 300 μm long feed-through is placed (3), after which the nozzle plate is reached. The nozzle plate is 75 μm thick and consists of a pyramid shaped funnel (4) and a nozzle (5) with a radius of 11 μm.

III. VISUALIZING IN THE INFRARED REGIME

In this research, the main challenge was to visualize the air bubble inside the ink channel. The MEMS ink channel is predominantly made out of silicon, which might facilitate infrared imaging, as silicon is transparent in near-infrared light at wavelengths of 1.1 μm up to 6 μm. This approach comes with quite an optical challenge, namely, the large difference in refractive index between silicon, the ink in the channel, and the air surrounding the printhead. When a wavelength of 1.2 μm is used, the refractive index n of silicon is approximately 3.5 times higher than that of air ($n = 1.0$). The ink used here is transparent in infrared light, but it has a much lower refractive index of $n = 1.5$. The consequences resulting from this difference become clear when the transmittance is described. Light can be represented by two orthogonal linearly polarized waves, one parallel and one orthogonal to the plane of incidence. The transmittances for these two polarizations are treated separately by the Fresnel equations[19]

$$T_{\perp} = \frac{n_t \cos\theta_t}{n_i \cos\theta_i} \left(\frac{2 \sin\theta_t \cos\theta_i}{\sin(\theta_i + \theta_t)} \right)^2, \quad (1)$$

$$T_{\parallel} = \frac{n_t \cos\theta_t}{n_i \cos\theta_i}\left(\frac{2\sin\theta_t \cos\theta_i}{\sin(\theta_i+\theta_t)\cos(\theta_i-\theta_t)}\right)^2. \quad (2)$$

Here θ_i gives the incident angle and n_i the refractive index of the incident media. In the transmissive media, the angle of refraction is given by θ_t with a refractive index n_t. If the light source is unpolarized, the transmittance is given by

$$T = \frac{T_{\perp} + T_{\parallel}}{2}. \quad (3)$$

When the incident light ray is perpendicular to the incident surface ($\theta_i = 0$), Eqs. (1) and (2) simplify to

$$T = T_{\perp} = T_{\parallel} = \frac{4n_t n_i}{(n_t + n_i)^2}. \quad (4)$$

Using these equations, the transmission curves for the silicon-ink and silicon-air interfaces can be calculated (Fig. 2). This shows that at the ink-silicon interface, at most 85% of the incoming light will be transmitted, and for the air-silicon interface only 70% of the light is transmitted. Figure 2 also shows a critical angle of incidence above which all light is reflected, termed total internal reflection.[19] For the silicon-air and the silicon-ink interfaces, the critical angles are 16.6° and 25.4°, respectively. Due to the critical angle, only limited optical access is obtained from within the inkjet channel, as is illustrated in Fig. 3. The left-hand part of the figure illustrates that all of the light that passes from the feed-through to the funnel will be reflected at the silicon-air interface. Even rays that enter the funnel surface at an angle of 89° still impinge on the nozzle plate at an angle of 25.4°, resulting in total reflection. The only possible way to visualize the inner channel is if the rays pass through parallel planes, as shown in the right-hand part of Figure 3.

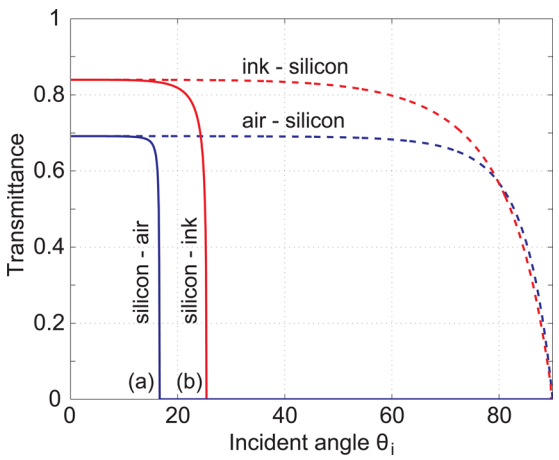

FIG. 2. (Color online) The unpolarized transmission curves for the silicon ink and silicon-air interfaces at a wavelength of 1.2 μm. The lower solid line gives the transmittance between silicon and air, the lower dashed line for the air-silicon interface, the upper solid line for the ink-silicon interface, and the upper dashed line for the silicon-ink interface. As the light travels from the ink through the silicon, 15% is reflected. Also, 30% of the light is lost at the silicon-air interface. The figure also shows at which angles total internal reflection occurs. For (a) the silicon-air interface, this is at 16.6°, and for (b) the silicon-ink interface it is at 25.4°.

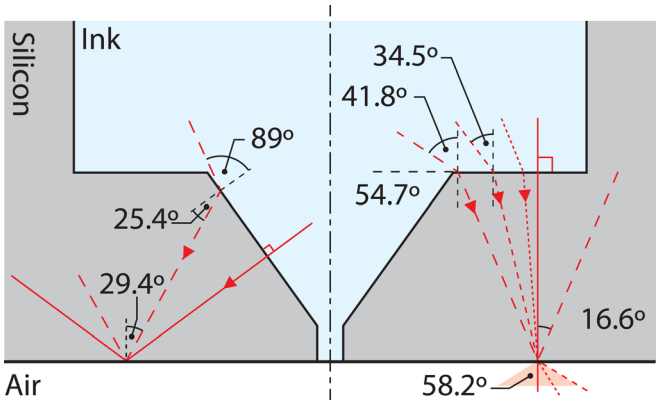

FIG. 3. (Color online) A ray trace of the light passing from the ink ($n = 1.5$) through the silicon nozzle plate ($n = 3.5$) to air ($n = 1.0$). In the left-hand panel it is shown that all of the light passing through the funnel area is refracted such that the light is fully reflected at the nozzle plate. In the right-hand panel, a sketch is given of the path traveled by the light when passing through parallel planes. Here the light that is incident under an angle of 41.8° is fully reflected at the nozzle plate. The NA of the microscope objective is 0.85, corresponding with an opening angle of 58.2°. Therefore, only the light that is incident to the silicon surface with an angle of 34.5° will be captured by the objective.

Illuminating the channel poses a similar challenge. As the channel is closely surrounded by neighboring channels, it is not possible to illuminate it from the sides. Also, illumination from above is not possible, as the upper part of the channel is covered by a piezo ceramic material. To overcome this problem, the channel can be illuminated from below, but again, only the light traveling perpendicular to the nozzle plate will be able to reach the inner part of the channel. This results in significant intensity loss, which can be compensated for by using a high-power infrared light source.

IV. EXPERIMENTAL PARAMETERS

Due to the limited optical access, reflected light microscopy is used, as it allows both the outgoing and the incoming light to enter the printhead through the same plane. For this purpose, an Olympus BX30MF microscope with an axial illumination unit (Olympus U-RLA) was used (Fig. 4). To illuminate the sample, a high intensity IR-light-emitting diode (LED) (Marubeni, L1200-66-60) was used. This light source has a radiant power of 60 mW with an intensity peak at a wavelength of 1.2 μm. By using a LED, illumination can be performed continuously as well as stroboscopically. An additional advantage of the LED is that, due to its narrow spectral bandwidth, chromatic abberation is minimized. The light from the LED is condensed into a narrow beam which reaches the microscope objective through a beam splitter. The objective has a magnification of 63× and a numerical aperture of 0.85. The reflected light from the sample is collected through the same microscope objective, passes through the beam splitter, and reaches the camera. The camera is an InGaAs camera (VDS Vosskühler, NIR-300) sensitive to wavelengths between 0.9 μm and 1.7 μm, with a pixel size of 30 μm and a maximum frame rate of 50 frames/s. Figure 5 shows a typical visualization of two inkjet channels facing each other. At the top and bottom of the image, the edges of the neighboring channels can be seen.

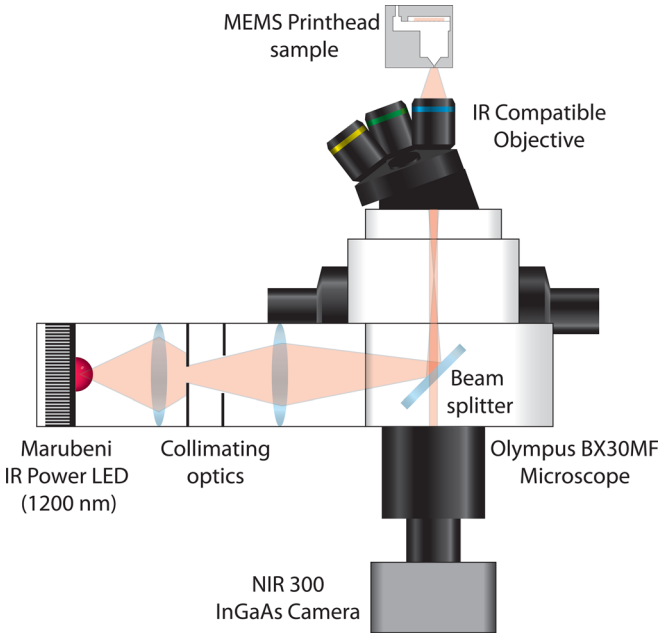

FIG. 4. (Color online) The reflected light setup that is used for infrared visualization of the MEMS inkjet channel. As a light source, a high intensity IR-LED with a wavelength of 1200 nm is used. A beam splitter is employed to reflect the light onto the objective. The light returning from the sample is gathered by the same objective and, after passing the beam splitter again, captured by the infrared camera.

In our experiments, we want to confirm that a bubble disrupts the drop formation and measure how its presence affects the acoustics. Therefore, the channel is operated at a very high, unstable frequency until the drop formation fails. The reflected light microscope setup is then used to visualize the presence, location, and size of the bubble

In order to capture the effect that an air bubble has on the channel acoustics, the acoustic signal and the visual recording have to be acquired simultaneously. The acoustics were measured by using the piezo not only as an actuator but also in receive mode. A similar technique was also applied in earlier work,[11,15,16] and a comparable technique was applied by Kwon *et al.*[20,21] The electronic circuit measured a

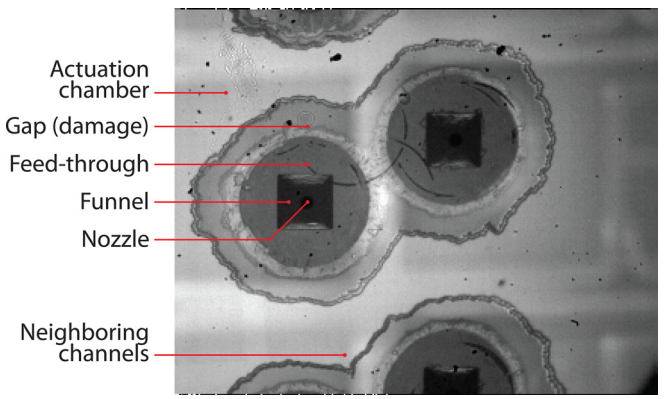

FIG. 5. (Color online) An infrared microscope image shows a MEMS printhead prototype from below. Two channels facing each other can be seen in the center of the image, clearly revealing the funnel and the feed-through section. In the back, even the actuation chamber is visible, but there is too little light passing through the nozzle area to illuminate this part. This particular sample shows a gray area around the nozzle, which is due to a lack of glue between the nozzle plate and the funnel.

relative change of the acoustics with respect to the normal operating conditions of the channel.

Two systems are studied here: a bubble dissolving inside the channel and a stable oscillating bubble. To study a dissolving bubble, first the bubble was entrapped. Then the actuation frequency was lowered to 2 Hz only to probe the acoustics in order to estimate the bubble's size. At this very low frequency, the bubble growth caused by rectified diffusion is negligible.[6–10] In order to prevent motion blur due to bubble oscillations, the channel was imaged just before the probing pulse. For each image, the LED was set to illuminate the channel for a typical length of 10 ms.

An oscillating bubble inside the channel was also studied. In this experiment, the bubble was entrapped, after which the actuation frequency was lowered to 20 kHz. The bubble moves to a preferred position and reaches an equilibrium size. If the actuation parameters remain constant, the bubble will stay fixed at this position for minutes without an effective change in volume. The extreme stability of the bubble oscillation gave the opportunity to use multiple short flashes at a fixed phase in the oscillation in order to create a single high contrast exposure. Each single image required 400 flashes of 300 ns each. By changing the time delay between the actuation and the illumination with steps of 0.5 μs, a stroboscopic movie of the bubble oscillation could be recorded.

V. MODELING THE PRINTHEAD

In order to understand how the bubble affects the channel acoustics, a one dimensional acoustic model was applied. This model calculates the propagation of acoustic waves in a viscous medium in a pipe with flexible walls. The piezo transmit transfer function is included in the model, and the channel acoustics at the piezo section are calculated in order to recover the electric response of the piezo. In the model, the printhead channel is treated as a number of axisymmetric coupled sections. The model also includes the two way coupling between the air bubble inside the channel and the channel acoustics. Inside the modeled geometry, the bubble can be positioned at any arbitrary location.

The dimensions of the model geometry were calculated by maintaining the same length and area for each section as in the MEMS printhead. The model also requires the electric expansion coefficient of the piezo, α, and the wall flexibility, β. These were determined using ANSYS 12,[22] giving $\alpha = 0.2$ pl/V and $\beta = 1.2$ pl/bar. For this geometry and the calculated parameters α and β, the piezo response can be calculated. Figure 6 shows the modeled acoustic signal and that of the experiment. Here the acoustic signal was calculated for a bubble with a radius of 11 μm, which corresponds to the optically measured value of 11 ± 1 μm. Thus we find excellent agreement between the measured and modeled acoustic pressure.

The model can be used to calculate the pressure and the flow rate in the individual channel sections and to calculate how the presence of the bubble influences these quantities. A more extensive treatment of this model can be found in Refs. 15 and 16.

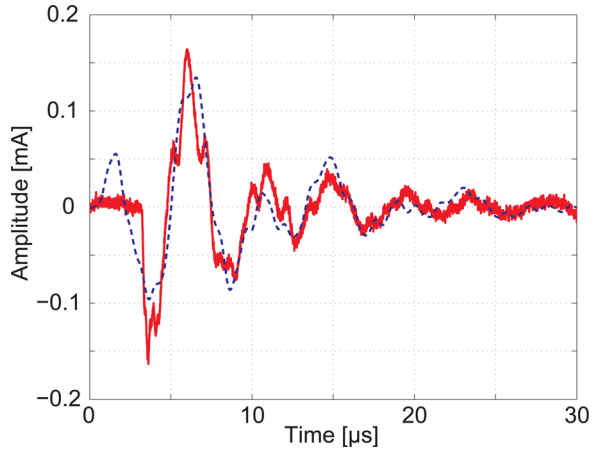

FIG. 6. (Color online) The acoustic signal calculated by the model (dashed line) compared with the acoustic signal from the experiment (solid line). In both the model and the experiment, an air bubble of 11 μm was present at the feed through-funnel crossing.

VI. RESULTS

Here the experimental results of the infrared recordings are presented, illustrating that infrared visualization is a valuable tool in researching disturbances inside the MEMS printhead. Similarly, the acoustic model can be utilized to predict the effect of disturbances on the acoustics. The validity of the model was tested by comparing the calculated results with the experimental results of a dissolving bubble and of an oscillating bubble. In the last section, the model is applied to calculate the effect of an air bubble on the velocity inside the nozzle.

A. Dissolving bubble

We recorded the dynamics of air bubbles entrapped inside the channel. Figure 7 shows a selection taken for a non-actuating case in which the bubble dissolves. This sequence was used to determine the radius R_{exp} of the bubble, as shown in Fig. 8. From these experiments it was found that a bubble with radius $R_{exp} = 12$ μm dissolves in approximately 30 s, corresponding to a volume of 0.3 pl/s, which is the same order of magnitude as was found in Ref. 16. The error analysis shown in Fig. 8 is derived from the image processing.

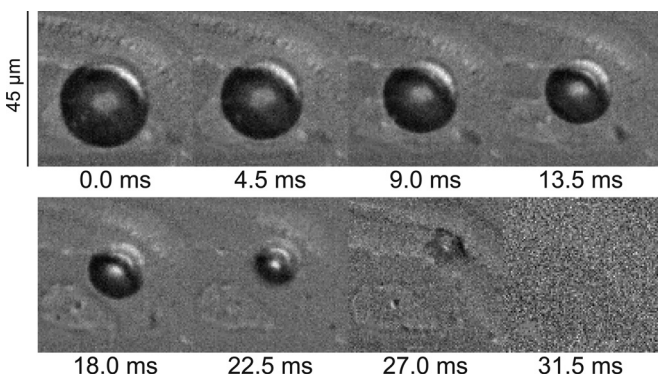

FIG. 7. A sequence of a bubble dissolving inside the ink channel. The initial bubble has a radius of 12 μm, and it fully dissolves in 30 s with an approximate dissolution rate of 0.3 pl/s.

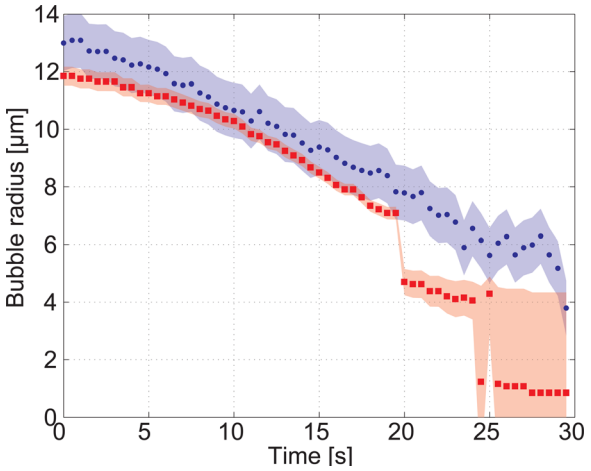

FIG. 8. (Color online) Using the infrared images, the bubble radii could be measured as a function of time (blue dots). The model was also used to predict the bubble radii, which are shown as red squares. The experimentally measured bubble radii agree with the calculated radii. After 22 s, the bubble is pushed into a slit, which could cause the deviation from the model at this point. The shaded area around the points depicts the error in both of these methods.

To calculate the bubble radius, the experimentally obtained acoustic signals (I_{exp}) were used in combination with the model. For that purpose, the model was set to calculate an acoustic signal (I_{mod}) for a certain bubble size (R_{mod}). The calculated signal was then compared with the experimentally obtained acoustic signal by calculating the relative norm of the difference ($\delta_i(R_{mod})$) given by

$$\delta_i(R_{mod}) = \frac{\|I_{exp} - I_{mod}(R_{mod})\|}{\|I_{exp}\|}. \quad (5)$$

Equation (5) is calculated by iteration over a range of bubble radii until δ_i reaches a minimum. The error in the calculation depends on the value of δ_i at this minimum and the sensitivity of δ_i to R_{mod}.[16]

Figure 8 shows the calculated bubble radius from multiple comparisons. Here we find good agreement between the model and the experiments until the bubble size decreases below 5 pl. Beyond this point, the modeled radius decreases significantly, which coincides with the bubble's movement into a slit between between the nozzle plate and the feed-through. The model is no longer applicable here, as the geometry at this position strongly deviates from the modeled geometry.

B. Oscillating bubble

The infrared experiments were also used to capture the radius as a function of time of an oscillating bubble, $R_{exp}(t)$. The pressure $P_{mod}(t)$ in the channel close to the bubble was calculated with the acoustic model, and the equilibrium bubble radius $R_{exp}(0)$ was used as an input parameter. The expected radius as a function of time $R_{RP}(t)$ is then calculated with the Rayleigh-Plesset equation, using the calculated channel pressure $P_{mod}(t)$ and the experimentally measured $R_{exp}(0)$ as input parameters. Figure 9 shows the radius calculated from the Rayleigh-Plesset equation $R_{RP}(t)$ compared with the experimentally measured radius $R_{exp}(t)$. The agreement is very good, considering that the error in the radius of

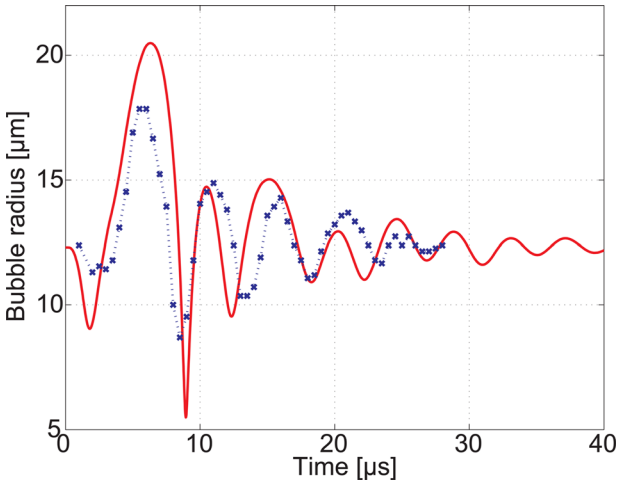

FIG. 9. (Color online) The oscillation of the bubble as measured from the experiment (dotted line) in comparison with the calculated oscillation (solid line). The oscillation is calculated with the full Rayleigh-Plesset equation, using the channel pressure calculated by the model.

the bubble is in the order of three microns. This error is caused mainly by the asymmetrical shape of the bubble as it is pushed into a corner of the channel. A movie of the oscillating bubble can be found online (Fig. 10).

C. Velocity inside the nozzle

In order to illustrate the applicability of the model, we now calculate the velocity of the fluid inside the nozzle during the actuation. Figure 11 shows the ink velocity inside the nozzle for different bubble radii during a single actuation cycle. In this example, the bubble is located 75 μm from the nozzle. It can be seen that as the bubble radius increases, the velocity of the ink in the nozzle decreases.

Figure 12 illustrates that as long as the bubble is within the nozzle, its position influences the velocity of the ink. The figure shows the maximum value of the velocity (U_{max}) of the ink for different bubble radii during an actuation cycle.

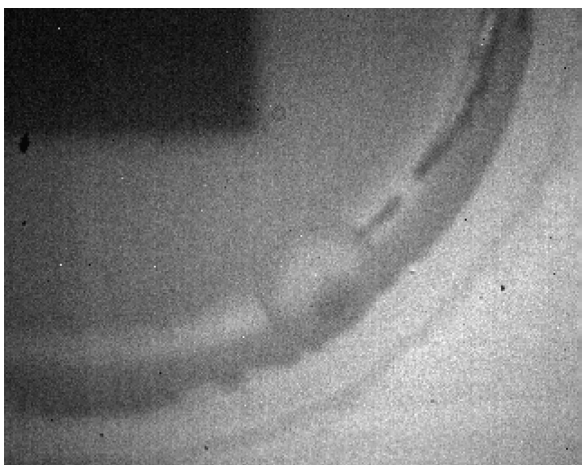

FIG. 10. A stroboscopic movie of an oscillation bubble inside the MEMS inkjet printhead. The oscillating bubble was imaged using an infrared light source. The mean bubble size in this recording is 12 μm (enhanced online) [URL: http://dx.doi.org/10.1063/1.3606567.1].

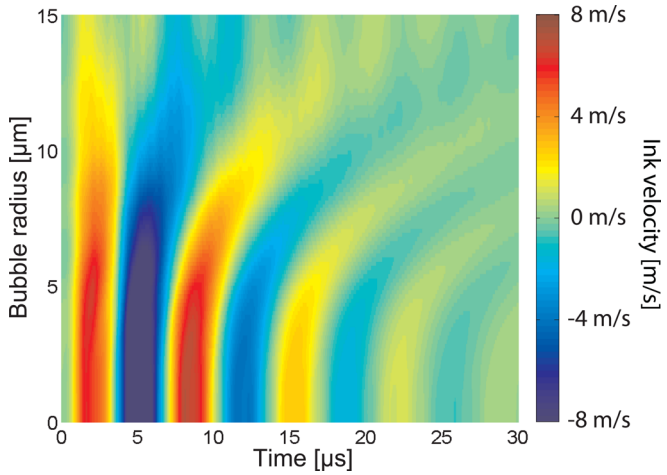

FIG. 11. (Color online) The model is applied to calculate the effect of an air bubble on the velocity dynamics inside the nozzle. Here the model was used to calculate the velocity amplitude during the first 30 μs after the actuation. The bubble was positioned 75 μm from the nozzle opening. A bubble smaller than 3 μm seems to have a small influence on the velocity amplitude. With increasing bubble size, the velocity amplitude in the nozzle decreases rapidly.

This figure also shows the root mean square value of the ink velocity (U_{rms}). It is interesting to note that if a small bubble ($R_{mod} \approx 5$ μm) is located close to the nozzle, the velocity in the nozzle increases. Therefore, if the bubble is entrapped close to the nozzle opening, an increase in the drop velocity could be expected just before the nozzle stops jetting. This was also observed in Ref. 11.

VII. SUMMARY AND OUTLOOK

In this research, the stability of a MEMS based piezo inkjet printhead was researched. By using an infrared

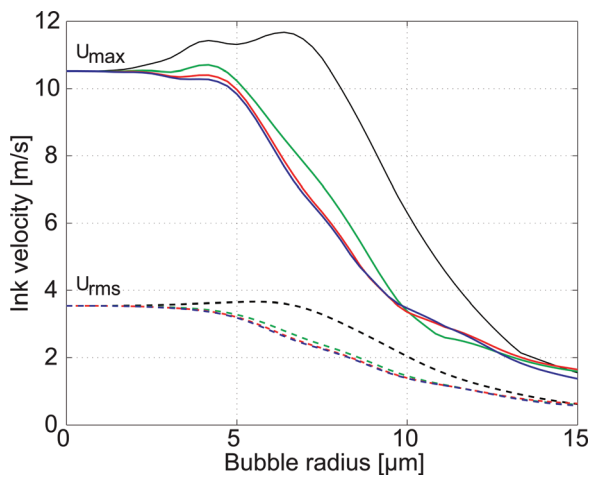

FIG. 12. (Color) The effect of the bubble on the velocity in the nozzle at different bubble positions. The solid lines represent the maximum velocity (U_{max}) in the nozzle during an actuation cycle. The dashed lines represent the root mean square of the velocity (U_{rms}). The black line represents a bubble positioned 25 μm from the nozzle, the green line a bubble 40 μm from the nozzle, the red line a bubble 75 μm from the nozzle, and the blue line a bubble 125 μm from the nozzle. Once the bubble passes beyond the nozzle, the overall effect is a decrease in the ink velocity. However, a small bubble close to the nozzle opening causes an increase in the velocity of the ink.

imaging technique, the presence of an air bubble inside the channel after the channel stopped jetting was confirmed. By using a high intensity infrared LED continuously, a dissolving bubble could be visualized. A novel illumination technique was introduced in which the high intensity infrared LED was used for the stroboscopic visualization of an oscillating bubble. Simultaneously with the visual recordings, the acoustics were measured and compared with a linear acoustic model. This could be used to calculate the bubble radius using the acoustical measurements, which agreed with the optical measurements. The pressure close to the bubble was calculated in order to predict the radial bubble dynamics, which corresponded very well with experimental values. It can therefore be concluded that the effect of the bubble is also correctly incorporated in the model.

The short calculation time of the model gives a wide range of possibilities, such as optimizing the acoustic design of the ink channel. In order to illustrate the importance of the numerical model, it was applied to calculate the effect of the bubble on the velocity dynamics inside the nozzle. Accurate and fast models will remain necessary in order to increase the knowledge of bubbles disrupting inkjet channels, and they can be used to further improve the reliability of inkjet printheads.

ACKNOWLEDGMENTS

This research could not have been conducted without help from Jan Simons (Océ Technologies B.V.), who designed the piezo current measurement system, and Ron Berkhout (Océ Technologies B.V.), who prepared the MEMS printhead sample. Part of this work was done in the II-A atomization research program of MicroNed, and the work was funded by Océ Technologies B.V. and MicroNed.

[1]M. Singh, H. M. Haverinen, P. Dhagat, and G. E. Jabbour, Adv. Mater. **22**(6), 673 (2010).
[2]H. Wijshoff, Phys. Rep. **491**(4–5), 77 (2010).
[3]E. Peeters, IEEE Comput. Sci. Eng. **4**(1), 44 (1997).
[4]C. Menzel, A. Bibl, and P. Hoisington, "MEMS Solutions for Precision Micro-Fluidic Dispensing Application," technical report, FUJIFILM Dimatix, Inc., 2004.
[5]J. de Jong, G. de Bruin, H. Reinten, M. van den Berg, H. Wijshoff, M. Versluis, and D. Lohse, J. Acoust. Soc. Am. **120**(3), 1257 (2006).
[6]C. E. Brennen, *Cavitation and Bubble Dynamics* (Oxford University Press, New York, 1995).
[7]T. G. Leighton, *The Acoustic Bubble* (Academic, London, 1994).
[8]S. Hilgenfeldt, D. Lohse, and M. Zomack, Eur. Phys. J. B **4**(2), 247 (1998).
[9]M. P. Brenner, S. Hilgenfeldt, and D. Lohse, Rev. Mod. Phys. **74**(2), 425 (2002).
[10]V. Garbin, B. Dollet, M. Overvelde, D. Cojoc, E. Di Fabrizio, L. van Wijngaarden, A. Prosperetti, N. de Jong, D. Lohse, and M. Versluis. Phys. Fluids **21**(9), 092003 (2009).
[11]J. de Jong, R. Jeurissen, H. Borel, M. van den Berg, H. Wijshoff, H. Reinten, M. Versluis, A. Prosperetti, and D. Lohse, Phys. Fluids **18**(12), 121511 (2006).
[12]J. Chung, C. P. Grigoropoulos, and R. Greif J. Microelectromech. Syst. **12**(3), 365 (2003).
[13]G. Han, J. C. Bird, K. Johan, A. Westin, C. Zhiqiang, and K. S. Breuer, Microscale Thermophys. Eng. **8**(2), 169 (2004).
[14]D. Liu, S. V. Garimella, and S. T. Wereley, Exp. Fluids **38**(3), 385 (2005).
[15]R. Jeurissen, J. de Jong, H. Reinten, M. van den Berg, H. Wijshoff, M. Versluis, and D. Lohse, J. Acoust. Soc. Am. **123**(5), 2496 (2008).
[16]R. Jeurissen, A. van der Bos, H. Reinten, M. van den Berg, H. Wijshoff, J. de Jong, M. Versluis, and D. Lohse, J. Acoust. Soc. Am. **126**(5), 2184 (2009).
[17]E. Bassous, H. H. Taub, and L. Kuhn, Appl. Phys. Lett. **31**(2), 135 (1977).
[18]Océ Technologies B.V., for more information on Océ CrystalPoint technology see http://global.oce.com/technologies/crystalpoint-technology.aspx.
[19]E. Hecht, *Optics*, 4th ed. (Pearson Education, New York, 2001).
[20]K. S. Kwon and W. Kim, Sens. Actuators, A **140**, 75 (2007).
[21]K. S. Kwon, Sens. Actuators, A **153**(1), 50 (2009).
[22]ANSYS CFD, For more information about ANSYS CFD see http://www.ansys.com/.